Maccaferri, F., Acocella, V., Rivalta, E. (2015): How the differential load induced by normal fault scarps controls the distribution of monogenic volcanism. - *Geophysical Research Letters*, *42*, 18, pp. 7507—7512.

DOI: http://doi.org/10.1002/2015GL065638

AGU PUBLICATIONS

Geophysical Research Letters

RESEARCH LETTER
10.1002/2015GL065638

Key Points:
- Monogenic cones at plate boundaries cluster on the footwall of normal fault scarps
- We simulate with numerical model dyke propagation under a scarp, accounting for crustal unloading
- Shallow dykes are steered to the fault footwall by scarp topographies down to the meter scale

Supporting Information:
- Supporting Information S1
- Table S1
- Figure S1
- Figure S2
- Figure S3
- Figure S4

Correspondence to:
F. Maccaferri,
francesco.maccaferri@gfz-postdam.de

Citation:
Maccaferri, F., V. Acocella, and E. Rivalta (2015), How the differential load induced by normal fault scarps controls the distribution of monogenic volcanism, *Geophys. Res. Lett.*, *42*, 7507–7512, doi:10.1002/2015GL065638.

Received 31 JUL 2015
Accepted 3 SEP 2015
Accepted article online 5 SEP 2015
Published online 30 SEP 2015

How the differential load induced by normal fault scarps controls the distribution of monogenic volcanism

F. Maccaferri[1], V. Acocella[2], and E. Rivalta[1]

[1]Helmholtz-Zentrum Potsdam Deutsches GeoForschungsZentrum GFZ, Potsdam, Germany, [2]Dipartimento Scienze, Roma Tre University, Rome, Italy

Abstract Understanding shallow magma transfer and the related vent distribution is crucial for volcanic hazard. Here we investigate how the stress induced by topographic scarps linked to normal faults affects the distribution of monogenic volcanoes at divergent plate boundaries. Our numerical models of dyke propagation below a fault scarp show that the dykes tend to propagate toward and erupt on the footwall side. This effect, increasing with the scarp height, is stronger for dykes propagating underneath the hanging wall side and decreases with the distance from the scarp. A comparison to the East African Rift System, Afar and Iceland shows that (1) the inner rift structure, which shapes the topography, controls shallow dyke propagation; (2) differential loading due to mass redistribution affects magma propagation over a broad scale range (10^0–10^5 m). Our results find application to any volcanic field with tectonics- or erosion-induced topographic variations and should be considered in any volcanic hazard assessment.

1. Introduction

Understanding eruption site distribution in monogenic fields is important for volcanic hazard, as eruptions occur over a wide area in contrast to central polygenetic volcanoes that have a main vent. The distribution of the monogenic volcanoes may be related to the availability of magma at depth, presence of discontinuities, the configuration of far– or near–stress field, as well as topographic loads [e.g., *Gudmundsson*, 2006; *Valentine and Krogh*, 2006; *Le Corvec et al.*, 2013]. In particular, topography may play an important role in creating a near–stress field capable of deflecting propagating dykes [*Fiske and Jackson*, 1972; *Acocella and Tibaldi*, 2005]. At the large scale, it has been suggested that crustal loading due to a volcanic edifice attracts ascending propagating dykes, creating the conditions for a polygenic edifice [*Dahm*, 2000; *Watanabe et al.*, 2002; *Kervyn et al.*, 2009; *Bonaccorso et al.*, 2010; *Maccaferri et al.*, 2011]. Moreover, unloading forces due to the creation of a graben depression were shown to have the potential to deflect ascending dykes to off-rift eruptions [*Maccaferri et al.*, 2014]. In all cases, the competition between loading/unloading forces and the driving pressure of the dykes controls how much dykes are deflected [*Watanabe et al.*, 2002]. These studies looked at large compressions/decompressions (several hundreds of meters to >1 km of added or missing topography) and spatial scales of the order of tens of kilometers. As for now, there are no studies focusing on small-scale topographic variations of 1 to 100 m.

Here we examine how shallow dyke propagation is affected by overlying topographic scarps created by tectonic extension within rift zones. These models are complementary to those of *Maccaferri et al.* [2014], as they provide a clue on the balance of the driving factors in the last few kilometers of the dykes' trajectory, where small-scale elements (1–100 m), such as individual fault scarp segments, may affect the location of vents. To this aim, we calculate the trajectories for shallow (<2 km) dykes ascending toward normal fault scarps. We simulate the stress field beneath the scarp by computing the stress change due to a step-like topography. We consider a lithostatic pressure proportional to the rock density ρ and include an extensional tectonic stress of intensity increasing with depth to simulate the weakness of the shallowest rock layers. The model results, and their consistency with several tens of natural examples, suggest that the control on dyke propagation exerted by loading and unloading is important for a broad range of process scales, and it should be considered in any evaluation of vent opening. Given the likely location of a magma reservoir, vent probability maps may be proposed depending on the scarp height.

2. Observations

We first consider the distribution of monogenic cones from the divergent plate boundaries within the southern part of the Kenya Rift, the Main Ethiopian Rift (MER), Afar, and Iceland (Reykjanes Peninsula and Northern

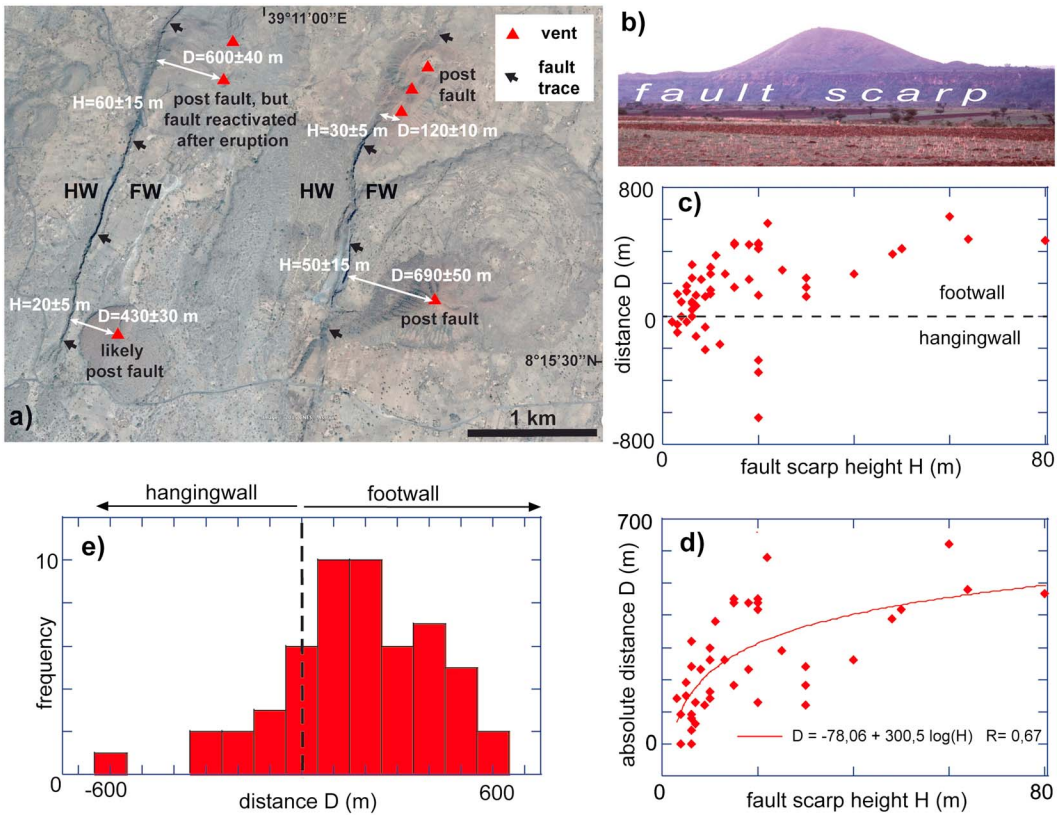

Figure 1. (a) Map view example of the spatial and temporal relationships between two major normal faults downthrowing to the west (black arrows) and volcanic vents (red triangles) through satellite images (Google Earth) along the central Main Ethiopian Rift (MER); the reported ages of the volcanoes relative to the faults have been evaluated considering any burial of the faults by the volcanic deposits. The distance *D* between a fault and the vent (positive if the vent is on the footwall FW, negative if vent is on the hanging wall HW) and the fault scarp height *H* are also included. (b) Field example of a monogenic vent developed on the footwall of a major normal fault with scarp height of ~50 m in the central MER. (c) Distribution of all monogenic cones as a function of the distance from a fault scarp *D* and the height of the scarp *H* (positive values are for cones on the footwall, negative for cones on the hanging wall). (d) Distribution of all monogenic cones on both the footwall and hanging wall as a function of the absolute distance from a fault scarp *D* and the height of the scarp *H*. (e) Frequency-distance *D* distribution of the cones regardless of the scarp height (derived from Figure 1c).

Volcanic Zone). We define the distance *D* of 54 monogenic basaltic volcanoes with regard to the closest normal fault scarp of height *H*: positive values of *D* refer to vents on the footwall side of the fault, whereas negative values to vents on the hanging wall side (downthrown part of the fault). In order to remove or minimize any effect from other fault scarps or topographic variations induced by volcanic activity, sedimentation, or erosion, we selected only the monogenic volcanoes nearby isolated active normal faults with sharp scarps, in areas of regular subhorizontal relief. Volcanic activity in these areas commonly postdates fault activity, as suggested by the volcanic deposits of the monogenic field usually overflowing the fault scarps (Figure 1a). The maximum distance considered for a volcano and the "nearby" scarp was of ±1 km, whereas the fault scarp height was between a few and 100 m. The data have been taken from field measurements (especially for fault scarps with smaller *H*; Figure 1b), topographic maps merged with high-resolution satellite images (especially for fault scarps with larger *H*) (Figure 1a). The error associated in evaluating the scarp height *H* is estimated as $<$30% of the measurement (this error is largely due to along-strike variations in the fault displacement) and that associated with the lateral distance *D* is $<$10% of the measurement (Figure 1a).

The considered natural cases of monogenic volcanoes nearby scarps show an overall proportion between the height of the fault scarp *H* and the distance from the fault *D* at which the monogenic cone is located, with the more distant volcanoes associated to larger fault scarps and predominantly located on the footwall (Figures 1c and 1d); this implies that the more distant volcanoes are associated to larger fault scarps. In addition, there is a predominant clustering on the fault footwall (74% of the data), peaking at a distance *D*

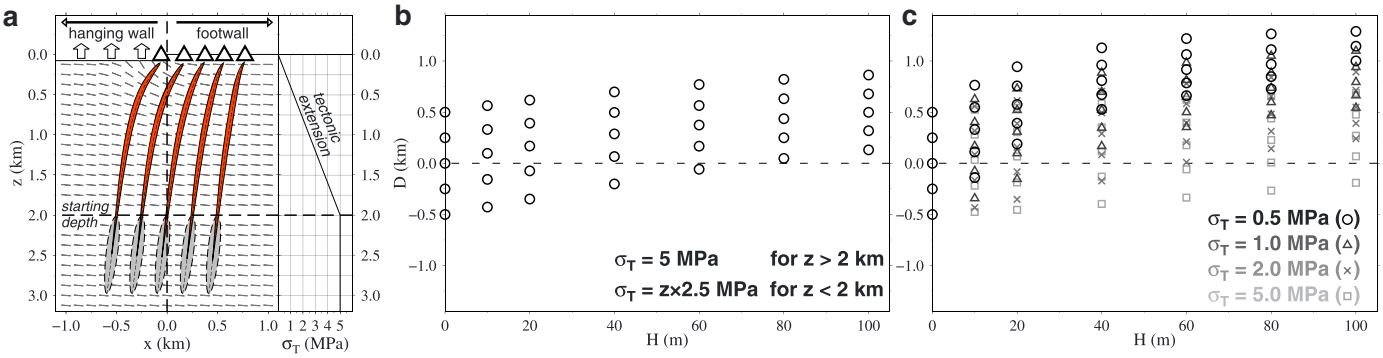

Figure 2. Results from numerical models; (a) dykes ascending from 2 km depth are driven toward the footwall of a 60 m scarp. Grey dashes represent the direction of σ_3 (minimum compressive axis) due to the unloading forces applied on the hanging wall (vertical arrows). Triangles represent the arrival position of dyke tips (D) at surface. The black curve in the right subplot represents the vertical profile assumed for the tectonic extension. (b) Distribution of dyke arrivals as a function of the distance from a fault scarp D and the height of the scarp H. (c) Same as Figure 2b with different values of uniform tectonic extension.

between 100 and 200 m from the fault scarp and gradually decreasing in frequency with distance (Figure 1e). The remaining 26% of the data peak at a distance $<$100 m from the fault scarp, gradually decreasing with the distance (Figure 1e).

3. Modeling

We investigate such a selective distribution of monogenic cones near fault scarps using a two-dimensional boundary element model [*Dahm*, 2000; *Maccaferri et al.*, 2010, 2011] to compute the trajectories of ascending dykes of initial cross-sectional area of 3×10^{-4} km^2 (equivalent to a volume ~6×10^{-4} km^3) from a depth $z=2$ km. The dykes are nucleated perpendicular to the minimum compressive stress σ_3. The trajectories are calculated by testing incremental elongations of the dykes in different directions and selecting the one maximizing the elastic and gravitational energy release [*Dahm*, 2000; *Maccaferri et al.*, 2010, 2011]. The dykes' initial position varies within a 1 km wide segment below the scarp, or $-0.5 > D_{in} > 0.5$ km where D_{in} is the initial horizontal distance from the scarp (Figure 2a). The dykes are boundary element mixed mode cracks in plain strain approximation composed by N contiguous and interacting dislocations, propagating in an elastic half space. The shear modulus of the host rocks is $G=12$ MPa and the Poisson's ratio $v=0.25$. The dykes open under assigned normal and shear stress given by the internal overpressure and by the shear component of the tectonic plus topographic stresses, respectively. The overpressure within the dyke is the difference between the magma pressure and the confining stress, which is the superposition of the lithostatic pressure (isotropic and depth dependent), the normal component of the topographic stress, and a far-field extensional tectonic stress. The fluid pressure is given by a magmastatic (linear) profile and accounts for magma compressibility, with a magma-rock density contrast of 300 kg/m^3. Such a density contrast guarantees the upward buoyant propagation of magma up to the surface. Lower buoyancy contrasts (~100 kg/m^3), possibly more realistic for basaltic magma intruding in Iceland, would have required either a larger volume of magma or additional overpressure from an active magma source in order for the dykes to reach the surface.

A fundamental input for the boundary element model is the state of stress of the crust, since dyke tends to orient perpendicular to σ_3. The tectonic stress, σ_T, increases linearly in the shallower 2 km, reaching a maximum value of 5 MPa at 2 km depth (Figure 2a). Such an assumption is meant to account for a progressively weaker shallow crust expected to be less and less capable of storing tension closer to the surface. Due to the high epistemic uncertainties in the values of the tectonic extension in nature, we additionally tested the effect of a constant tension with different magnitudes in the range of 0.5 to 5 MPa (see Figure 2c). The stress induced by the scarp topography is computed by applying unloading forces of intensity ρgH on the scarp hanging wall (Figure 2a). In such a way, we account for the local contribution of the scarp to the overall stress change linked to the formation of a wide graben-like structure [*Maccaferri et al.*, 2014]. In other words, the scarp topography represents a discontinuity in the unloading forces linked to the surface mass redistribution induced by tectonic extension. Therefore, the fault scarp can be seen as the boundary of a depression of depth H, and the unloading forces at the boundary determine the local stress field beneath the scarp. Such a stress change involves both a rotation of the principal stresses and a variation of their relative ratio.

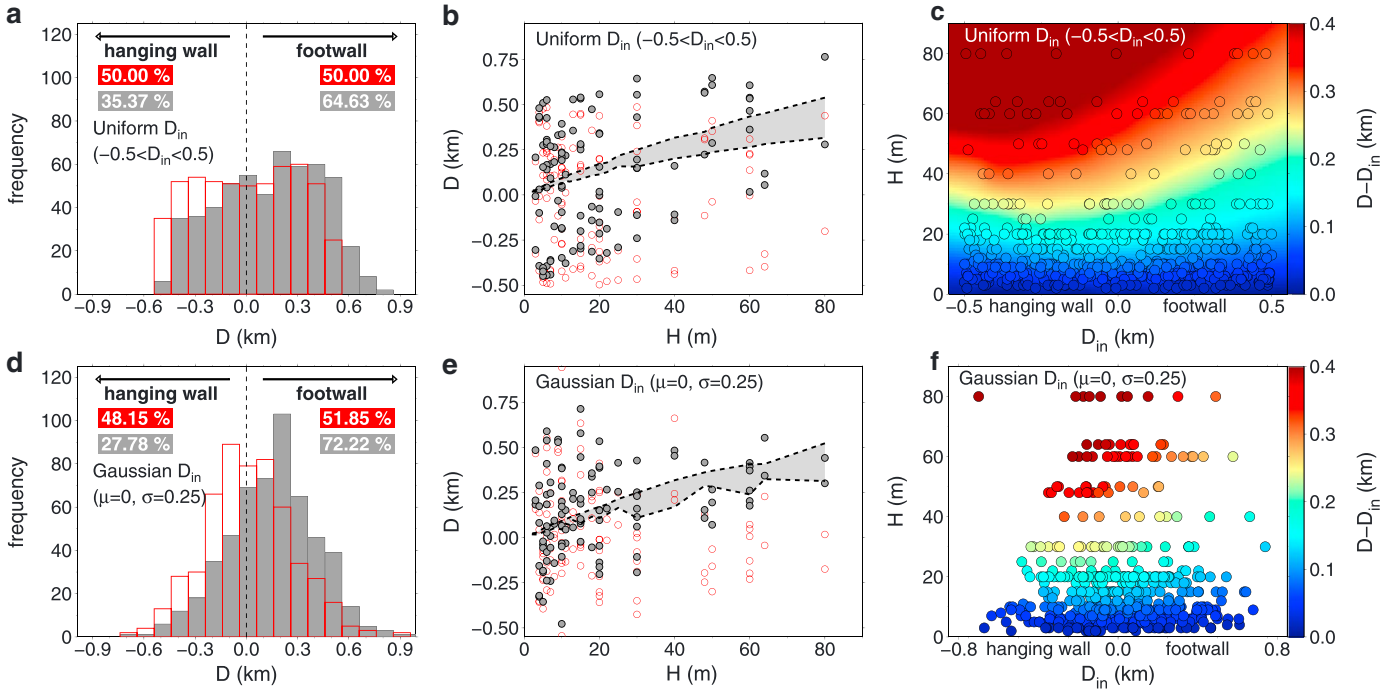

Figure 3. (a) Frequency-distance distributions. In red the distribution of initial dyke positions (D_{in}) and in grey the distribution of dyke arrival positions at surface (D). The distribution used for D_{in} is uniform. (b) Initial distances D_{in} (red circles) and distances from the scarp after arrival at surface (grey circles) for dykes propagating under the effect of different scarp heights H; the light grey area bounded by two black dashed lines represents the maximum and minimum horizontal deviations ($D_{in} - D$) exhibited by dykes for different scarp height H. Only 20% of the numerical results have been plotted as grey and red circles for reasons of clarity. (c) ($D_{in} - D$) color coded as function of D_{in} and H. (d–f) The same as Figures 3a–3c with a Gaussian distribution for D_{in}. For each case (uniform and Gaussian D_{in}) we considered a sample of propagating dykes equal to 10 times the observations (540 dykes propagating under the 54 scarp heights measured in the field).

We compute this by using analytical formulas for a uniform surface unloading acting over the scarp base [*Davis and Selvadurai*, 1996; *Dahm*, 2000, Appendix A]. In general, this stress field depends on the depth, H, and width, W of a topographic feature. For the present application H corresponds to the scarp height, while W is large enough that the local stress field in the vicinity of the scarp (±1 km) remains stable. We find stability for $W > 5$ km, and therefore, we fix $W = 10$ km. In the model we do not consider the presence of multiple scarps, as the observations have been collected nearby isolated active normal faults.

In our model runs, we vary the unloading force as ρgH and test different distributions of the initial horizontal distances of the dyke upper tips from the scarp (D_{in}). We test the following: (1) symmetric distribution at constant intervals: $D_{in} = [-0.5; -0.25; 0; 0.25; 0.5]$ km (five dykes for each of the six tested scarp heights, Figures 2b and 2c); (2) uniform random distribution in the range $-0.5 < D_{in} < 0.5$ km (10 dykes for each of the 54 measured scarp heights, 540 dykes in total, Figures 3a–3c); (3) Gaussian random distribution with mean $\mu = 0$ and standard deviation $\sigma = 0.25$ km (10 dykes for each observation, Figures 3d–3f). For the first case—symmetric initial distribution of dykes at depth—we also test different values of a constant uniform far-field tectonic extension (0.5, 1, 2, and 5 MPa). In each model run, the dykes were not interacting with each other or with previous dykes. We also tested the influence of the initial dip of the dyke, forcing the intrusions to start as perfectly vertical dykes. The results do not change significantly; see Figure S1 in the supporting information. We find that the dykes tend to systematically deviate toward the footwall. The deflection depends on the amount of rotation of σ_3 induced by the unloading forces in the vicinity of the scarp (Figure 2a). The effect is stronger for higher scarps and for dykes that start closer to the scarp (Figure 2b), while it tends to vanish for lower scarp heights and at large offset from the scarp. For higher scarp heights and lower extensional tectonic stresses, the distribution of dyke arrivals at the surface is progressively displaced toward the footwall side ($D > 0$), and the dykes emerge at the surface closer to each other (Figure 2c).

In order to compare directly the numerical results with the observations from Figure 1c, we set H equal to the value of each of the 54 observations and for each H we run 10 models uniformly (case 2, Figure 3a) and normally distributed (case 3, Figure 3d). We also plot D and $D - D_{in}$ as a function of H (Figures 3b and 3e), finding

a trend similar to the observations (Figure 1b). Finally, the deviation $D - D_{in}$ as a function of D_{in}/H (Figures 3c and 3f) shows that dykes originated under the hanging wall are deviated more than those originated under the footwall. These plots confirm that the amount of deviation decreases for increasingly positive and increasingly negative D_{in}.

4. Discussion and Conclusions

The distribution of monogenic cones at divergent plate boundaries resulting from several tens of measurements collected in ideal conditions (isolated scarps) highlights clustering of cones on the fault footwall. In particular, the higher the fault scarp, the more distant the cone from the fault scarp on the footwall. This selective distribution suggests that the propagation path of the dykes feeding the cones may be deflected in the vicinity of fault scarps and that fault scarps do not necessarily represent a preferential pathway for ascending dykes, at least toward the surface.

The similarities between the observations and the model results suggest that the stress field induced by crustal unloading applied at the hanging wall of the scarp is the primary explanation for the clustering of the studied volcanic cones at the footwall. Particularly, we find notable agreement in the comparison between Figures 3a–3d and Figure 1c (numerical and observed frequency-distance distributions). Moreover, it seems that the Gaussian distribution for D_{in} (Figure 3d) fits better than the uniform one, reproducing a peeked maximum in the frequency at about 0.1–0.2 km and a fast decay for higher (positive) and lower (negative) D (as in Figure 1c). The uniform distribution of D_{in} (Figure 3a) does reproduce the maximum at 0.2 km, but the maximum is less peeked and the decay slower than in Figure 1c. We repeated the numerical experiments several times, in order to appreciate how random perturbations of the initial dyke distribution affect the final result (some examples are given in Figure S2, supporting information). The uniform distribution of D_{in} resulted in more variability in the results, producing frequency-distance histograms that visually reproduce the observations as well as histograms looking quite different.

We find an overall good agreement between models and observations in the trend of D as a function of H (Figures 3b–3e and Figure 1c). The main difference between observations and numerical experiments is the scatter of D for low values of H: from the numerical results we would expect scattered arrivals (Figure 3e) while the observations show more focused arrivals close to low scarps (Figure 1c). Fault planes or preexisting structures may induce additional stresses and capture dykes [e.g., *Valentine and Krogh*, 2006], possibly explaining the higher clustering of the vents near low fault scarps in nature. Moreover, any high-angle fault plane increases the extent of the footwall at depth, enhancing any capturing effect of the fault plane on the dyke [*Gaffney et al.*, 2007]. These two factors have not been considered in our models (where, in order to isolate the effect of the scarp topography on the dyke propagation, we do not consider any structural discontinuity) and could possibly explain the slight discrepancy between numerical results and observations. Additionally, the discrepancy may reflect an initial distribution of D_{in} more concentrated around $D_{in} = 0$, with respect to what we tested. Indeed, we can better reproduce the lack of scattering in D for low H just by reducing our numerical samples close to the number of observations, in the hypothesis of an initial Gaussian distribution. The resulting distribution of D versus H for this case is shown in Figure S3 (supporting information). Because of the reduced numerical sample, these distributions are more subjected to statistical fluctuations, so that some random generations result in a better match with the observations (e.g., Figure S3a) and others in a larger scattering of D for low H (e.g., Figures S3b and S3c).

The numerical results, overall well consistent with the observations, suggest that shallow dyke propagation in areas characterized at a large scale by a relatively regular, flat surface may be affected by the presence of scarps. The degree of this capturing effect depends mainly on the height of the scarp, so that higher scarps deflect dykes more efficiently toward the footwall side of the fault.

This relationship, which is valid at the 1–100 m scale complements what was previously found at the 10 to 100 km scale, explaining the presence of off-rift volcanoes [*Maccaferri et al.*, 2014]. This indicates that the crustal loading or unloading due to the activity of one or more sets of normal faults is an efficient mean to control the shallow propagation of magma, in the form of dykes, at several scales of observations. More supporting evidence can be found also at the intermediate scale (200–700 m) of the Limagne fault, Chaine de Puys, where the increased frequency of vents on the fault footwall correlates with the better developed fault scarp (Figure S4).

Our results are applied to monogenic cones within divergent plate boundaries along the East African Rift System, Afar, and Iceland, chosen because of the presence of active and sharp fault scarps on a generally subhorizontal surface. However, as loading and unloading processes have been proven to result from sharp topographic variations, we suggest that a similar mechanism may also affect the propagation of dykes in any area characterized by important scarps within volcanic areas. These include monogenic cones in strike-slip or contractional settings, where the fault scarp may be still related to a significant dip-slip (normal or reverse for strike-slip faults, reverse for contractional faults) component of motion. Flat areas characterized by selective erosion or deposition, producing clear, straight, and isolated scarps, independently of any tectonic activity, may also deflect propagating dykes accordingly to our models. Therefore, our results may also widely apply to convergent plate boundaries and intraplate magmatism characterized by important tectonic structures, or simply to flat areas characterized by deposition or sedimentation.

Our results, of wide applicability, testify the general importance of topography in controlling the shallow transfer of magma, complementing previous studies highlighting the importance of volcanic ridges in focusing volcanic activity [e.g., *Fiske and Jackson*, 1972] of calderas in reorienting dykes [*Munro and Rowland*, 1996] and of sector collapse in attracting [*McGuire et al*., 1990; *Tibaldi*, 2003] or deflecting radial dykes [e.g., *Acocella and Tibaldi*, 2005; *Walter et al*., 2005; *Delcamp et al*., 2012].

Finally, our results may be helpful in volcanic hazard assessment, to consider the possible opening of vents during the rise of a dyke toward the surface, especially in volcanic areas characterized by the lack of a central edifice with strong topographic expression. Dyke-induced seismicity could be used to pinpoint the position of the intrusion and asses whether the dyke is most likely to erupt in a certain area. The most promising areas to apply our results include flat zones of monogenic volcanism, caldera complexes largely filled by deposits or water, and shield volcanoes with very gentle slopes.

Acknowledgments

We thank the Editor, Andrew Newman, and the reviewers Francesco Mazzarini and Benjamin Van Wyk de Vries who helped in improving this manuscript with their constructive comments. We thank Benjamin Van Wyk de Vries for providing the observations from the Limagne fault and Figure S4. This work was funded by a PRIN 2009 project (VA responsible) and by the European Union through the ERC StG CCMP-POMPEI, grant agreement 240583, and the Supersite MED-SUV project, grant agreement 308665.

The Editor thanks Francesco Mazzarini and Benjamin van Wyk de Vries for their assistance in evaluating this paper.

References

Acocella, V., and A. Tibaldi (2005), Dike propagation driven by volcano collapse: A general model tested at Stromboli, Italy, *Geophys. Res. Lett.*, *32*, L08308, doi:10.1029/2004GL022248.

Bonaccorso, A., G. Currenti, C. Del Negro, and E. Boschi (2010), Dike deflection modelling for inferring magma pressure and withdrawal, with application to Etna 2001 case, *Earth Planet. Sci. Lett.*, *293*(1), 121–129.

Dahm, T. (2000), Numerical simulations of the propagation path and the arrest of fluid-filled fractures in the Earth, *Geophys. J. Int.*, *141*(3), 623–638.

Davis, R., and A. Selvadurai (1996), *Elasticity and Geomechanics*, Cambridge Univ. Press, Cambridge.

Delcamp, A., V. R. Troll, B. V. W. de Vries, J. C. Carracedo, M. S. Petronis, F. J. Pérez-Torrado, and F. M. Deegan (2012), Dykes and structures of the NE rift of Tenerife, Canary Islands: A record of stabilisation and destabilisation of ocean island rift zones, *Bull. Volcanol.*, *74*(5), 963–980.

Fiske, R. S., and E. D. Jackson (1972), Orientation and growth of Hawaiian volcanic rifts: The effect of regional structure and gravitational stresses, in *Proceedings of the Royal Society of London A: Mathematical, Physical and Engineering Sciences*, vol. 329, pp. 299–326, The Royal Society, London.

Gaffney, E. S., B. Damjanac, and G. A. Valentine (2007), Localization of volcanic activity: 2. Effects of pre-existing structure, *Earth Planet. Sci. Lett.*, *263*(3), 323–338.

Gudmundsson, A. (2006), How local stresses control magma-chamber ruptures, dyke injections, and eruptions in composite volcanoes, *Earth Sci. Rev.*, *79*(1), 1–31.

Kervyn, M., G. G. J. Ernst, B. van Wyk de Vries, L. Mathieu, and P. Jacobs (2009), Volcano load control on dyke propagation and vent distribution: Insights from analogue modeling, *J. Geophys. Res.*, B03401, doi:10.1029/2008JB005653.

Le Corvec, N., K. B. Spörli, J. Rowland, and J. Lindsay (2013), Spatial distribution and alignments of volcanic centers: Clues to the formation of monogenetic volcanic fields, *Earth Sci. Rev.*, *124*, 96–114.

Maccaferri, F., M. Bonafede, and E. Rivalta (2010), A numerical model of dyke propagation in layered elastic media, *Geophys. J. Int.*, *180*(3), 1107–1123.

Maccaferri, F., M. Bonafede, and E. Rivalta (2011), A quantitative study of the mechanisms governing dike propagation, dike arrest and sill formation, *J. Volcanol. Geotherm. Res.*, *208*(1), 39–50.

Maccaferri, F., E. Rivalta, D. Keir, and V. Acocella (2014), Off-rift volcanism in rift zones determined by crustal unloading, *Nat. Geosci.*, *7*(4), 297–300.

McGuire, W. J., A. D. Pullen, and S. J. Saunders (1990), Recent dyke-induced large-scale block movement at Mount Etna and potential slope failure, *Nature*, *343*(6256), 357–359.

Munro, D. C., and S. K. Rowland (1996), Caldera morphology in the western Galápagos and implications for volcano eruptive behavior and mechanisms of caldera formation, *J. Volcanol. Geotherm. Res.*, *72*(1), 85–100.

Tibaldi, A. (2003), Influence of cone morphology on dykes, Stromboli, Italy, *J. Volcanol. Geotherm. Res.*, *126*(1), 79–95.

Valentine, G. A., and K. E. Krogh (2006), Emplacement of shallow dikes and sills beneath a small basaltic volcanic center–The role of pre-existing structure (Paiute Ridge, southern Nevada, USA), *Earth Planet. Sci. Lett.*, *246*(3), 217–230.

Walter, T. R., V. Acocella, M. Neri, and F. Amelung (2005), Feedback processes between magmatic events and flank movement at Mount Etna (Italy) during the 2002–2003 eruption, *J. Geophys. Res.*, B10205, doi:10.1029/2005JB003688.

Watanabe, T., T. Masuyama, K. Nagaoka, and T. Tahara (2002), Analog experiments on magma-filled cracks: Competition between external stresses and internal pressure, *Earth Planets Space*, *54*(12), e1247–e1261.